Geological Society, London, Special Publications Online First

Geophysical characterization of the upper crust in the transitional zone between the Pampean flat slab and the normal subduction segment to the south (32–34°S): Andes of the Frontal Cordillera to the Sierras Pampeanas

M. Sánchez, F. Lince Klinger, M. P. Martinez, O. Alvarez, F. Ruiz, C. Weidmann and A. Folguera

Geological Society, London, Special Publications, first published February 6, 2014; doi 10.1144/SP399.12

Geophysical characterization of the upper crust in the transitional zone between the Pampean flat slab and the normal subduction segment to the south (32–34°S): Andes of the Frontal Cordillera to the Sierras Pampeanas

M. SÁNCHEZ[1]*, F. LINCE KLINGER[1], M. P. MARTINEZ[1,2], O. ALVAREZ[1], F. RUIZ[2], C. WEIDMANN[1] & A. FOLGUERA[3]

[1]*CONICET. Instituto Geofísico y Sismológico Ing. Volponi, Universidad Nacional de San Juan, Ruta 12, km. 17, CP 5407, San Juan, Argentina*

[2]*Instituto Geofísico y Sismológico Ing. Volponi, Universidad Nacional de San Juan, Ruta 12, km. 17, CP 5407, San Juan, Argentina*

[3]*Department Cs. Geol. FCEN. U.B.A. Buenos Aires, Inst. Estudios Andinos 'Don Pablo Groeber', Argentina*

**Corresponding author (e-mail: 1marcossanchez@gmail.com)*

Abstract: The Nazca Plate subducting beneath the South American Plate has strongly influenced Cenozoic mountain growth in western Argentina and Chile sectors (32–34°S; 70–66°W). At these latitudes, the Pampean flat slab has induced the development of prominent mountain systems such as the Frontal Cordillera, the Precordillera, and the associated Sierras Pampeanas in the eastwards foreland region. Through a gravity study from the Frontal Cordillera to the Sierras Pampeanas region between 32 and 34°S, we delimit a series of geological structures that are accommodating shortening in the upper crust and others of regional and subsurface development, without any clearly defined mechanics of deformation. Additionally, through an isostatic residual anomaly map based on the Airy-Heiskanen local compensation model, we obtain a decompensative gravity anomaly map that highlights anomalous gravity sources emplaced in the upper crust, related to known geological structures. In particular, by applying the Tilt method which enhances the gravity anomalies, the NW-trending Tunuyan Lineament is depicted south of 33.4°S following previous proposals. Using the decompensative gravity anomaly, two profiles were modelled through the northern sector of the study area using deep seismic refraction lines, borehole data and geological information as constraints. These density models of the upper crust of this structurally complex area accurately represent basin geometries and basement topography and constitute a framework for future geological analysis.

At the transitional zone between the Pampean flat subduction zone and the normal subduction system located immediately to the south, the area between the Frontal Cordillera and the Sierras Pampeanas is of great interest due to the existence of crustal discontinuities, attributed to sutures between different allochthonous and parautochthonous Palaeozoic terranes (Ramos *et al.* 2002). These lithospheric blocks are known as the Pampia, Cuyania and Chilenia terranes and constitute the Andean basement at these latitudes (latitude 27–33°S). Basin development is thought to have been influenced by reactivation of these basement discontinuities in Late Triassic and Early Cretaceous times; understanding the anatomy of this system is important for geological analyses.

Located in the north-central region of Argentina, the Pampia terrane collided (according to certain hypotheses) with the Rio de la Plata craton during latest Proterozoic–Early Cambrian time (Ramos & Vujovich 1993; Brito Neves *et al.* 1999; Almeida *et al.* 2000). This led to deformation, metamorphism and magmatism (González Bonorino 1950; Caminos 1979; Casquet *et al.* 2008) exposed in the Pampean Orogen beyond the area of interest.

To the west, the Cuyania exotic microcontinent detached from Laurentia during Cambrian time collided in Late Ordovician time with western Gondwana (Thomas & Astini 2003). Its definition is based on fauna, palaeomagnetic position and isotopic and geochemical composition (Abbruzzi *et al.* 1993; Benedetto & Astini 1993; Kay *et al.* 1996; Rapalini & Astini 1997; Benedetto *et al.* 1999; Keller 1999; Ramos 2004). However, a parautochthonous origin was proposed for it in other studies (Aceñolaza *et al.* 2002; Finney *et al.* 2003;

From: Sepúlveda, S. A., Giambiagi, L. B., Moreiras, S. M., Pinto, L., Tunik, M., Hoke, G. D. & Farías, M. (eds) *Geodynamic Processes in the Andes of Central Chile and Argentina*. Geological Society, London, Special Publications, **399**, http://dx.doi.org/10.1144/SP399.12

Peralta *et al.* 2003). During the amalgamation of Cuyania – which potentially occurred during the Famatinian orogenic cycle (Late Ordovician) (Rapela *et al.* 2001) – magmatism affected the western sector of the Sierras Pampeanas in La Rioja province (Pankhurst *et al.* 1998; Quenardelle & Ramos 1999) and to the south in the Sierra de San Luis (Llambías *et al.* 1996).

Mesoproterozoic basement, attributed to the Cuyania exotic microcontinent, is exposed in the Western Sierras Pampeanas. In particular, in the Sierra Pie de Palo the basement is thrust on top of an Early Cambrian carbonate platform in metamorphic facies, considered laterally equivalent to the Precordillera sedimentary facies (Ramos *et al.* 1986; Ramos 1988, 1995; Vujovich *et al.* 2004). According to these hypotheses, Mesoproterozoic rocks exposed in this region would have had a complex evolution prior to its final amalgamation with the Gondwana supercontinent, in which a suprasubduction system would have accreted in the Greenvillian Orogen showing typical mid-ocean ridge and island-arc basalt (MORB and IAB) components. Alternative models have considered Sierra de Pie de Palo basement as part of the proto-Andean margin (Galindo *et al.* 2004) and, even as an independent block, amalgamated to Cuyania before the Ordovician (Mulcahy *et al.* 2007).

In the Precordillera, limestones and associated siliciclastic successions belonging to this terrane are exposed as a thin-skinned fold-and-thrust belt that to the south merges in a thick-skinned belt (Ramos 1995; Ramos *et al.* 1998).

Most of these crustal discontinuities, potentially related to sutures between different terranes, have suffered extensional reactivations in Late Triassic and Early Cretaceous times. The Cuyo basin constitutes one of the Late Triassic rift systems that intersect the Andean trend obliquely with a predominant NW orientation. Eastern-most depocentres are sparse over the foreland area beneath thick sections of Cenozoic synorogenic strata (Uliana & Biddle 1988; Legarreta *et al.* 1993), while those at the orogenic wedge in the west were selectively incorporated during Andean growth stages. These Late Triassic depocentres are related to the initial stages of the western Pangea break-up, while the Cretaceous depocentres are spatially and temporally associated with the Paraná hotspot that affected the early Atlantic margin (Boll & de la Colina 1993; Lagorio 2008).

In particular, the south-western section of the Sierras Pampeanas corresponding to the Sierra del Gigante and Sierra de las Quijadas has been the locus of a Cretaceous rift system which led to the accumulation of within-plate volcanic rocks interfingered with continental facies (Rivarola & Spalletti 2006; Martinez *et al.* 2012).

Between the eastern Precordillera and Sierras Pampeanas, the Jocoli basin registers Andean exhumation as a frontal foredeep due to the flexure of the eastern Cuyania block (Fig. 1a).

The western and central sectors of the Precordillera in the Pampean flat slab segment (Baldis & Chebli 1969; Baldis *et al.* 1982) are composed of typical east-vergent thin-skinned thrust sheets (Allmendinger *et al.* 1990; von Gosen 1992). Contrastingly, the eastern Precordillera and Sierras Pampeanas to the east are thick-skinned blocks with opposite vergences (Bracaccini 1946; Rolleri & Baldis 1969; Ortiz & Zambrano 1981; von Gosen 1992; Zapata & Allmendinger 1994; Zapata & Allmendinger 1997).

These two systems interfere at a triangular thick-skinned zone (Zapata & Allmendinger 1994, 1996). South of Mendoza city, this triangular zone disappears at the zone where the inclination of the Wadati–Benioff zone increases, passing to a normal subduction zone (Figueroa & Ferraris 1989).

The Jocoli basin is partially located on that triangular zone (Cominguez & Ramos 1991). Its infill records the beginning of the uplift of the Frontal Cordillera that began at *c.* 15 Ma (Bercowski *et al.* 1993). Afterwards, the basin records the uplift of the Sierra de Pedernal in the Precordillera simultaneously to the uplift of the Western Sierras Pampeanas to the east (Ramos *et al.* 1997).

The aim of this paper is to make a density model that reflects the structure and basin geometry in this transition zone from a flat to a normal subduction zone (32–34°S and 70–66°W; Fig. 1a), using a large database of high-quality gravity data, boreholes and deep seismic refraction lines, constrained with pre-existing geological models in the area. The model will describe Andean anatomy at this key area, a valuable tool in structural, basin and tectonic studies.

Methodology

Database

This study is based on a dataset which comprises 23 680 gravity stations that are the property of the Geophysical Seismological Institute of the National University of San Juan (IGSV). The dataset covers the central region of Argentina in an area between 27.5° and 36.5°S and from 71° to 65°W, extending outside of the boundaries of our study area in order to avoid border effects. The spatial distribution of gravity stations from the original sources is shown in Figure 1b.

This database was measured using geodetic gravimeters with precisions of ± 0.1 mGal. In order to ensure the accuracy of the measurements and to homogenize all stations obtained on different

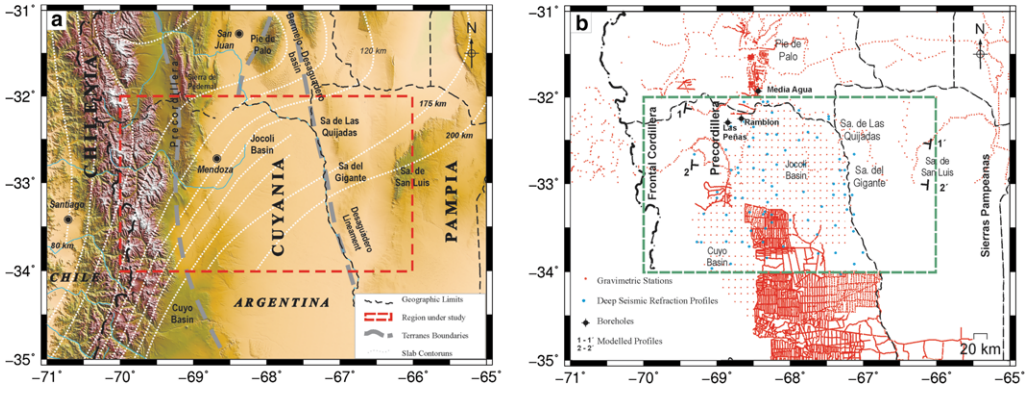

Fig. 1. (**a**) Digital elevation model (DEM 90 m × 90 m) that indicates the study area (red box) in a complex zone characterized by the transition from a flat subduction zone of the Nazca plate in the north, to a normal subduction segment. Nazca plate isodepth contours obtained by Alvarado *et al.* (2007) are represented by white dotted lines. The proposed boundaries between Palaeozoic terranes are indicated by grey dashed lines (see text for references). (**b**) Geophysical databases available in the region of study. Green dashed line: area under study; red dots: gravity data courtesy of Instituto Geofísico Sismológico Volponi (IGSV); light blue dots: deep seismic refraction data available in the area by Yacimientos Petroliferos Fiscales (YPF) boreholes. 1–1′: Modelled profiles in Figures 9 and 10.

campaigns, each gravity station has been linked to the national altimetry network. This process allows any possible artefact due to problems in the levelling of the different sources to be avoided, as all were referred to the IGSN 71 network (International Gravity Standardization Net 1971) and linked to the fundamental station Miguelete (Buenos Aires) through the nodal 145 City of San Juan and PF9 into the N24 line (Morelli *et al.* 1974). More details about the homogenization and reductions to the altimetry network are provided in Villella & Pacino (2010). This methodology allows a proper data reduction to be performed for anomaly calculation using classical corrections detailed below (Blakely 1995; Hinze *et al.* 2005).

The theoretical or normal gravity accounting for the mass, shape and rotation of the Earth is the predicted gravitational acceleration on the best-fitting terrestrial ellipsoidal surface. We have used the latest ellipsoid recommended by the International Union of Geodesy and Geophysics: the 1980 Geodetic Reference System (GRS80) (Moritz 1980). The Somigliana closed-form formula (Somigliana 1930) for theoretical gravity g_T on this ellipsoid at latitude (south or north) φ is:

$$g_T = \frac{g_e(1 + k\sin^2\varphi)}{\sqrt{1 - e^2\sin^2\varphi}}, \qquad (1)$$

where the GRS80 reference ellipsoid has the value g_e of 978 032.67715 mGal, where g_e is normal gravity at the equator; k of 0.001931851353 where k is a derived constant; and e^2 of 0.0066943 800229, where e is the first numerical eccentricity.

The height correction is called the free-air correction and is based on the elevation (or orthometric height) above the geoid (sea level) rather than height above the ellipsoid. The revised standards use the ellipsoid as the vertical datum rather than sea level. Conventionally, the first-order approximation formula of Δgh in milligal, where gravity anolamy $\Delta g = 0.3086$, is used for this correction.

The Bouguer correction accounts for the gravitational attraction of the layer of the Earth between the vertical datum (i.e. the ellipsoid) and the station. This correction, ΔgB in milligals, is traditionally calculated assuming that the Earth between the vertical datum and the station can be represented by an infinite horizontal slab with equation:

$$\Delta gB = 2\pi G\sigma h = 4.193 \times 10^{-5}\sigma h \qquad (2)$$

where G the gravitational constant is $6.673 \pm 0.001 \times 10^{-11}$ m^3 kg^{-1} s^{-2} (Mohr & Taylor 2001) and σ is the density of the horizontal slab (kg m^{-3}). The mean used density is 2670 kg m^{-3} (Hinze 2003), and h is the height of the station (m) relative to the ellipsoid in the revised procedure or relative to sea level in the conventional procedure.

The terrain correction adjusts the gravity effect produced by a mass excess (mountain) or deficit (valley) with respect to the elevation of the observation point. The terrain correction was obtained using two digital elevation models, a local and a regional DEM. Software program OASIS v.7.2 combines the algorithms developed by Kane (1962) and Nagy (1966), where elevation models were obtained from the Shuttle Radar Topography

Mission (SRTM) of the United States Geological Survey (USGS). Through the use of a sampling procedure, the corresponding topographic correction value was assigned to each gravity station. The resulting maximum error for this correction was ± 1.8 mGal. Finally, the complete Bouguer anomaly values (Fig. 2) were calculated on a regular grid cell size of 5×5 km using the minimum curvature method (Briggs 1974).

Isostatic anomaly

The 'regional' flexural compensation models proposed by Watts *et al.* (1995), Tassara *et al.* (2007), Wienecke *et al.* (2007), Pérez-Gussinyé *et al.* (2008) and Tassara & Echaurren (2012) for the Central Andes have enabled the determination of equivalent elastic thickness variables that are progressively higher eastwards in the foreland area, beyond the magmatic arc locus associated with the subduction process in the west. However, crustal thickening in the hinterland of the Central Andes, where the arc is located and was hosted (Introcaso *et al.* 1992*b*), can be explained by relative low values of the effective elastic thickness which justify the use of a 'local' compensation model (Airy–Heiskanen) in the study area.

This assumption has already been applied in this region by several authors with fairly good results (Götze & Evans 1979; Introcaso *et al.* 1992*a*; Chapin 1996; Götze & Kirchner 1997; Whitman 1999; Introcaso *et al.* 2000; Tassara & Yáñez 2003).

In order to obtain the isostatic root, we performed the calculation of the Airy–Heiskanen model frame using different parameters (see Table 1). We have taken into consideration other models integrating (1) gravity with seismic data; (2) the global model presented by Assumpção *et al.* (2013); and (3) the Moho depths determined by Gans *et al.* (2011) using receiver functions (see Fig. 3). Finally, the isostatic root that best fits with the above models was calculated using the following parameters: normal thickness crust $T_n = 40$ km; contrast density $\rho = 400$ kg m^{-3} and density crust $\rho = 2670$ kg m^{-3}. This T_n value was found by Christensen & Mooney (1995) as the mean global crustal thickness. The adopted crust–mantle density contrast ($\rho_{cm} = 400$ kg m^{-3})

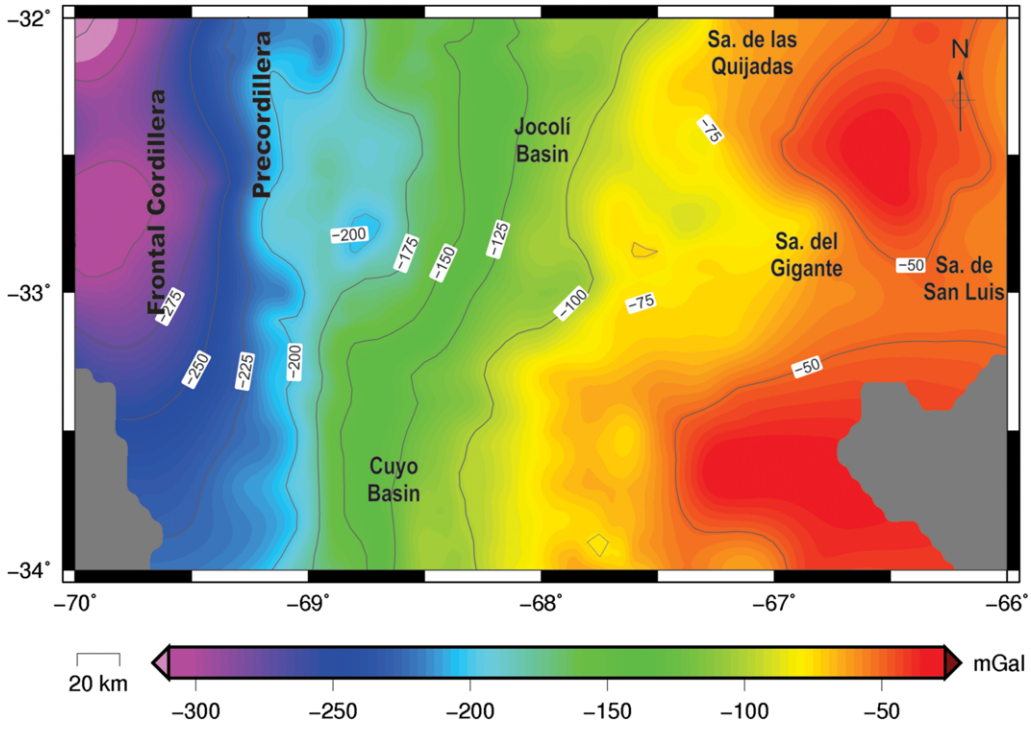

Fig. 2. Bouguer anomaly map obtained from 23 680 stations of terrestrial gravity data. The Bouguer anomaly values were calculated on a regular grid cell size of 5×5 km, using the minimum curvature method. To the west at Frontal Cordillera, the negative effect of the Andean root has a clear influence on the gravity signal; the effect of this decreases towards the east at Sierras Pampeanas.

Table 1. *Parameters used in the isostatic root calculation*

Crustal thickness (km)	T_{n1}	30
	T_{n2}	35
	T_{n3}	40
Contrasts of crust–mantle interface densities (kg m^{-3})	ρ_{cm1}	330
	ρ_{cm2}	350
	ρ_{cm3}	400
Topographic load density (kg m^{-3})	ρ_{ct}	2670

was used previously by Martinez *et al.* (2006) and Gimenez *et al.* (2009).

With the exception of the south-western edge of Figure 3 (where there is a lack of data), there exists a good correspondence between the depths determined by the hydrostatic Moho model with the solutions (coloured dots) obtained by Gans *et al.* (2011). Likewise, our results are consistent with depths found by the global model presented by Assumpção *et al.* (2013). The comparison is plotted with dashed white lines on Figure 3. For this case, we observed a trend deepening to the west (with the exception of isoline 40*).

Using the Moho hydrostatic geometry (Fig. 3), the isostatic gravity root effect was calculated (Fig. 4). This map presents a high negative gravity gradient ranging from −25 to −275 mGal. By subtracting the gravity effect of the isostatic root from the Bouguer anomaly (Figs 2 & 4), an isostatic residual anomaly is obtained (Fig. 5). These residual anomalies could mask short-wavelength anomalies, generated from more superficial sources (Simpson *et al.* 1986).The isostatic corrections could therefore be used to partially remove the effect of the crustal roots produced by the topographic elevations and depressions. Nevertheless, they fail to resolve the problem when the crustal roots are derived from high-density crustal regions with or without topographic expression. To overcome this drawback, we apply the decompensative gravity anomaly technique as proposed by Cordell *et al.* (1991).

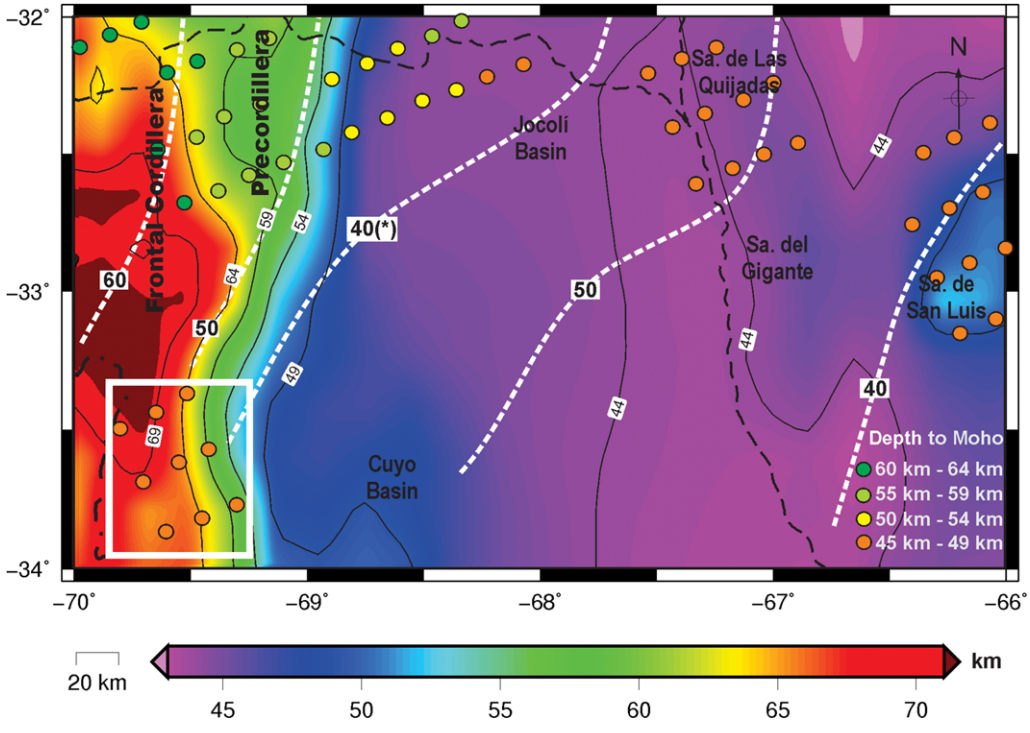

Fig. 3. Depth of mantle–crust interface corresponding to the geometry of the computed hydrostatic Moho in the region of study. Circular dots represent the differences between the Moho depth obtained by Gans *et al.* (2011) and the gravimetric results, and dashed white lines represent the differences between a global model by Assumpção *et al.* (2013) and the gravimetric results. Our results present a general good fit with the Gans *et al.* (2011) results, with the exception of the region within the white rectangle. Assumpção *et al.* (2013) results are also consistent with our results, with a deeper root under the Andes and a shallowing trend towards the east (with the exception of 40*).

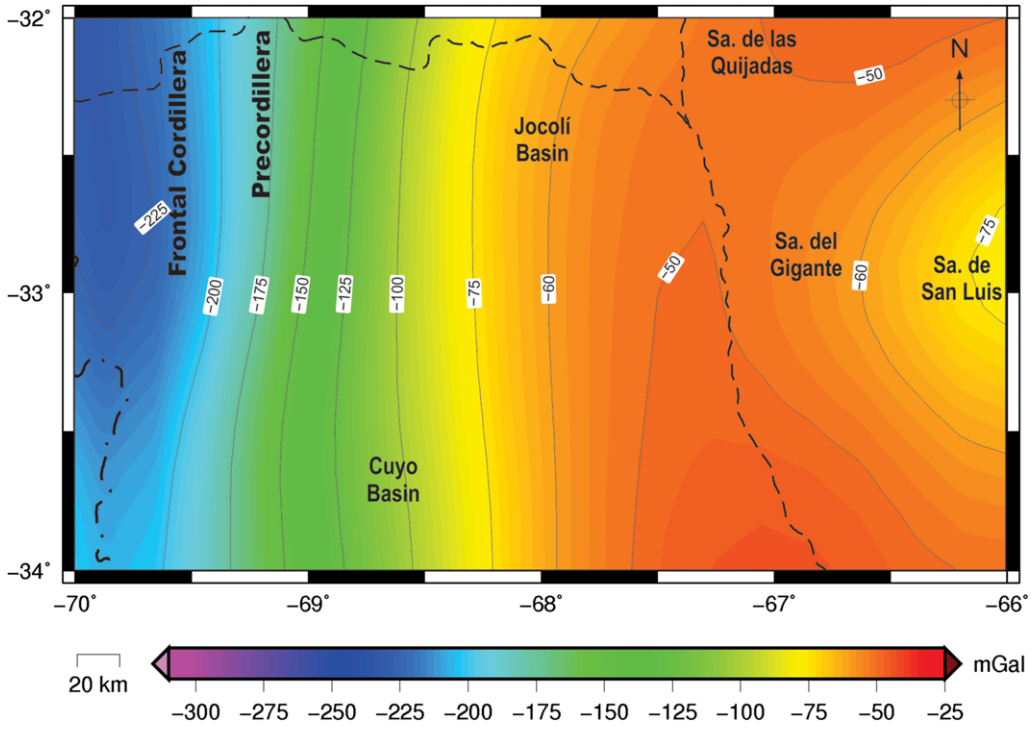

Fig. 4. Gravity response of isostatic root. Isoanomalies decreasing to the west indicate the importance of the horizontal component of the Andean root. Recall that the gravity effect of the root is equal and opposite to the isostatic correction.

Decompensative gravity anomaly

A 'decompensative' correction to the isostatic gravity anomaly also allows us to remove the gravity effect of isostatic compensation of geological loads. Under a hypothesis of local (as opposed to regional) compensation, the gravity effect of a shallow mass can be separated from the effect of gravity of a geological body emplaced on upper crust by its deep compensating root. The decompensative anomaly is the Bouguer gravity anomaly with isostatic and decompensative corrections added. The decompensative correction (Cordell *et al.* 1991) is calculated based on the upwards continuation of the isostatic anomaly (AI) in order to minimize the effects of the short-wavelength structures. The decompensative anomaly is then obtained by subtracting the regional anomaly (upwards continuation) from the isostatic anomaly (AI).

In this work we apply a variant of this procedure (Cordell *et al.* 1991), working with the power spectrum method of the isostatic anomaly instead of performing an upwards continuation in order to separate the different wavelengths (Fig. 6) through the proposed transformation by Mishra & Naidu (1974).

The above-mentioned improvement allows a depth value of the sources causing anomalies to be estimated; average depths of the anomalous sources are then determined, as proposed by Spector & Grant (1970). Additionally, spectral analysis determines the cut-off frequency for long wavelengths and applies the filter more efficiently.

As indicated, the lower frequencies of the power spectrum indicate an approximate depth of 20 km. This value coincides with the décollement of the main contractional structures determined for this region by Cominguez & Ramos (1990) using deep seismic reflection data. These results were confirmed by Gilbert *et al.* (2006) using receiver functions. The décollement of the fold-and-thrust belt are located in a brittle-ductile transition that could constitute a natural discontinuity, where magmas associated with Late Triassic–Early Cretaceous rifting stages reside temporally or permanently, constituting an anomalous mass in the middle–upper crust.

To fulfil the objective of studying structures shallower than 20 km above this mass anomaly area, we used a high-ass filter with a cut-off wave number k_c of 0.022 cyc km^{-1} (Fig. 6). Using this cut-off parameter, we obtained the decompensative isostatic residual anomaly map (Fig. 7).

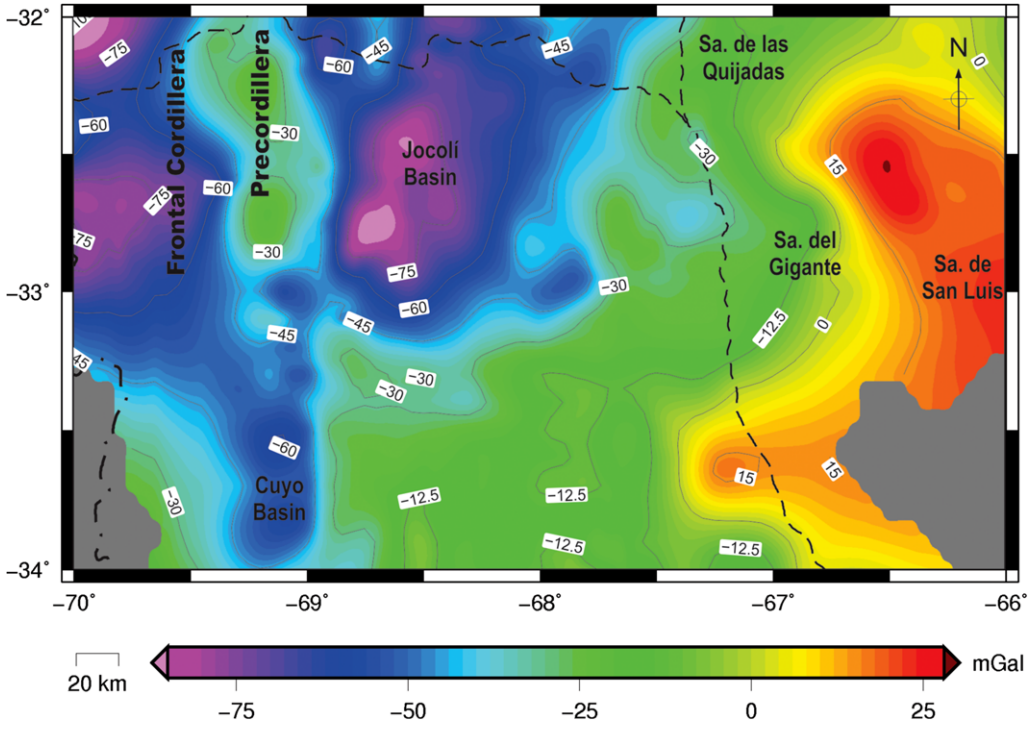

Fig. 5. Map of isostatic residual anomaly computed by subtracting the gravity isostatic root (Fig. 4) from the Bouguer anomaly map (Fig. 2).

Enhancement of anomalies: Tilt method

The Tilt method is effective in enhancing the edges of bodies that generate anomalous effects in the gravity field, assuming a vertical contact model. This method uses the horizontal and vertical gradients of the gravity field, and does not require previous knowledge about the geometry. The Tilt

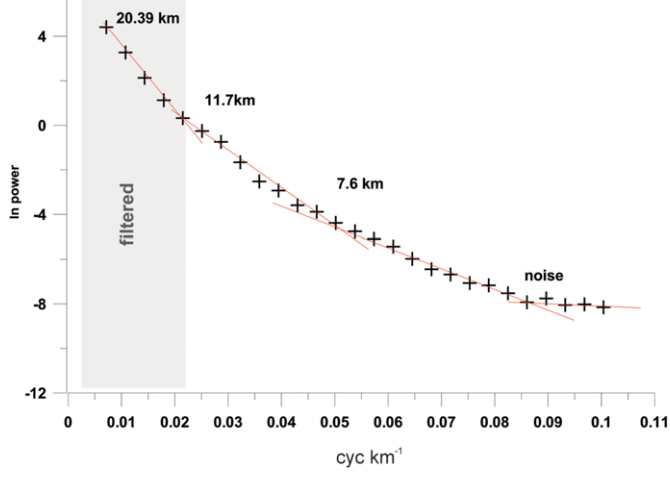

Fig. 6. Power spectrum of the radial isostatic anomaly obtained from the proposed transformation of Mishra & Naidu (1974). The isostatic anomaly input signal is used. Numbers in kilometres indicate the average depths obtained for each line. The shaded area indicates the filtered frequency range.

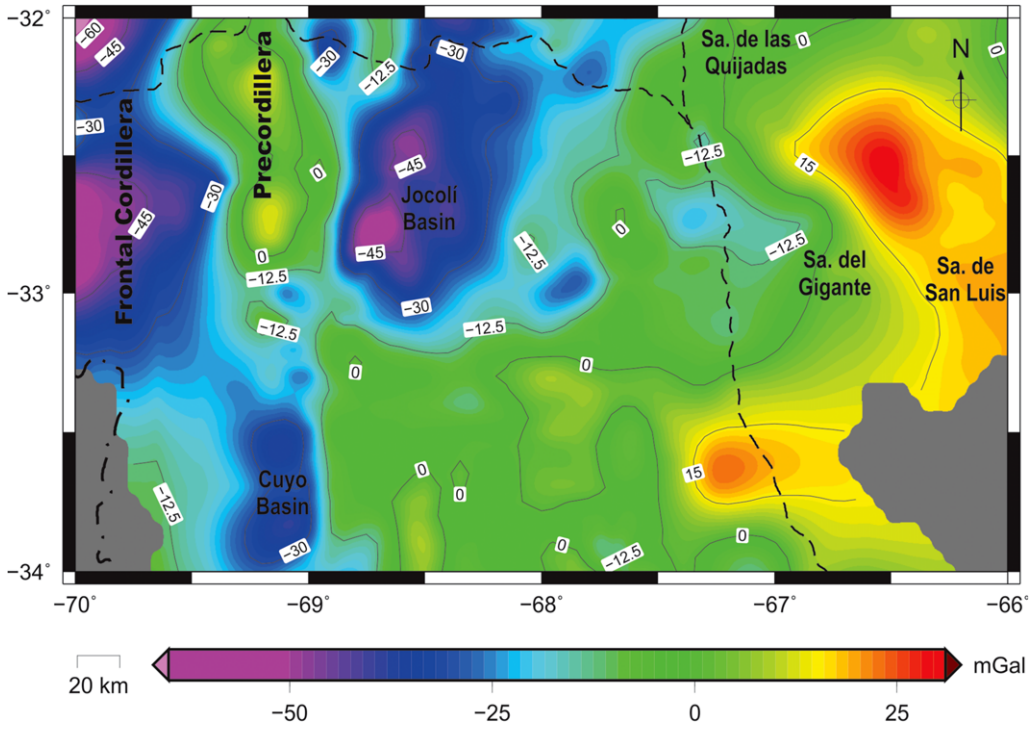

Fig. 7. Decompensative gravity anomaly map. Even although this map is morphologically similar to Figure 5, the range of values is different and physically represents residual anomalies of shallow sources.

method has therefore been applied with success to highlight edges and shapes of geological structures (e.g. Salem *et al.* 2008; García Torrejón *et al.* 2011; Oruç & Selim 2011). The tilt angle (Miller & Singh 1994; Thurston & Smith 1997; Verduzco *et al.* 2004) is defined:

$$\text{Tilt} = \arctan\left(\frac{T_{zz}}{\sqrt{T_{xz}^2 + T_{yz}^2}}\right) \qquad (3)$$

where the denominator represents the horizontal gravity gradient and T_{zz} is the vertical gravity gradient. Figure 8 depicts the results obtained by applying this method. From this analysis two regional structures with an unknown direct significance are identified: the San Pedro Ridge and the Tunuyan Lineament that are subsequently described.

2D models

In order to relate the gravity signal to the potential basement segmentation observed in the decompensative gravity anomaly map and the Tilt map, we constructed two density models over selected NW-trending profiles (Fig. 7). Constraints used in these models are deep seismic refraction lines, borehole data and geological information (Fig. 1b).

The initial reference model is a simple two-layer model which includes depth of the basement and sediments, which fill the basins. We then improved the model by introducing potential lateral density variations between the basements of Cuyania and Pampia terrains. Variable sediment densities are assigned for each basin based on log constraints (see following section). From these models we obtained the direct gravity response. Finally, the difference between observed data and the calculated response was minimized varying the geometry of the polygons from the original model using a 2D forward modelling algorithm (Talwani *et al.* 1959; Marquardt 1963).

Geophysical constraints

Densities used to model profiles have been taken from oil exploration borehole data, corresponding to Las Peñas log (YPF.SJ.Sp.EP.-1) located within the Jocoli basin (Fig. 1b). To determine the mean density of the sedimentary basin filling, we obtained the weighted averaged densities of each lithological unit (by estimating its thickness). We found a mean density value of 2390 kg m^{-3}, which

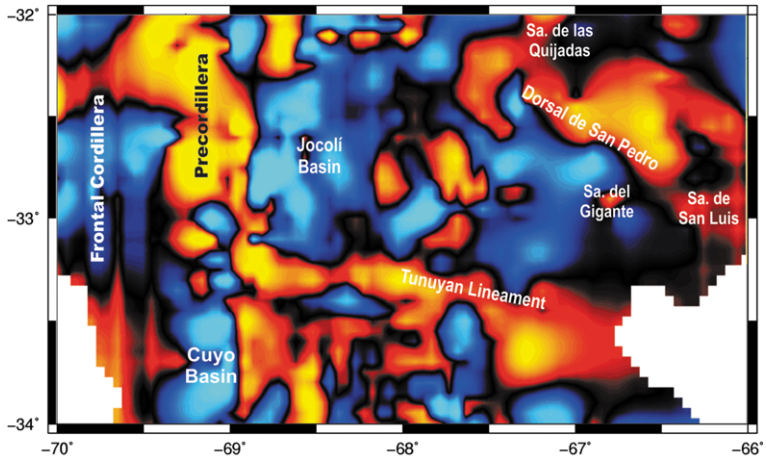

Fig. 8. Application of the Tilt method on the isostatic residual anomalies map. This method allows enhancement of the edges and shapes of geological structures that generate anomalous effects in the gravity field, assuming a vertical contact model from the horizontal and vertical gradients of the gravity field. The high gradient located south of 33.4°S latitude trending approximately westwards is associated with the Tunuyan Lineament, identified by Kostadinoff & Gregori (2004). This feature, which has no surface expression, has been associated with the boundary between two regions with different seismotectonic behaviour, possibly associated with the change in the Nazca plate subduction angle (Perucca & Bastias 2005).

is similar to the density value of 2400 kg m^{-3} proposed by Azeglio *et al.* (2010) towards the east of the neighbouring Las Salinas basin. In order to obtain the crystalline basement density, we used the velocities obtained from deep seismic refraction data available in the area from Yacimientos Petroliferos Fiscales (YPF). By means of the Gardner equation (Gardner *et al.* 1974) we determined a range of density values from 2676 to 2716 kg m^{-3} corresponding to velocities from 5600 to 6000 m s^{-1}. These velocity values are similar to those of the crystalline basement in Western Sierras Pampeanas found by Snyder *et al.* (1990).

The geometry of the crystalline basement along the profiles was adjusted using information obtained from: (1) seismic refraction data (YPF); (2) seismic sections interpreted by Cominguez & Ramos (1990) and Vergés *et al.* (2007) between Precordillera and Sierras Pampeanas; and (3) surficial data from Western Sierras Pampeanas (Snyder 1990; Zapata & Allmendinger 1996).

Profile 1

This profile was traced in the northern region over 340 km (see location on Fig. 1b). This section cut across the Eastern Precordillera, the Jocoli basin and the northern part of Sierra de las Quijadas (Western Sierras Pampeanas). The profile crosses the Salinas basin up to the NW border of the Sierra de San Luis. The gravity model obtained along this section was adjusted through deep seismic refraction profiles, borehole records and geological information available on this zone (Fig. 9). The western border was modelled using a triangular structural geometry determined by overthrusts with opposite vergences proposed previously (Figueroa & Ferraris 1989; Ramos *et al.* 1997). In Cerro Salinas, a series of thrust sheets are detached from the contact between the sedimentary section and the basement producing a west-vergent structure as described by Vergés *et al.* (2007).

The Jocoli basement geometry ($\rho_{cb} = 2670$ kg m^{-3}) is characterized by faulted blocks that have a strong gravimetric contrast with the basin fill ($\rho_{sed} = 2390$ kg m^{-3}). The highest sedimentary infill (*c.* 3 000 m) is located to the east of Cerro Salinas, diminishing towards the Sierra de las Quijadas (up to 1500 m). Eastwards in the Western Sierras Pampeanas a pronounced increase in the gravity residual anomaly is observed (Fig. 7). This anomaly has been linked to potential mafic bodies buried at the contact zone between the Cuyania and Pampia terrains (Introcaso & Pacino 1987; Ramos 1994; Miranda & Introcaso 1999; Gimenez *et al.* 2000; Martinez *et al.* 2007). This was resolved by modelling the crust assigned to the Pampia terrain with a higher density ($\rho = 2720$ kg m^{-3}). In this model the Salinas basin with a sedimentary thickness of 1 km and a mean density of 2400 kg m^{-3} therefore has a basement constituted by the Pampia terrain (Azeglio *et al.* 2010).

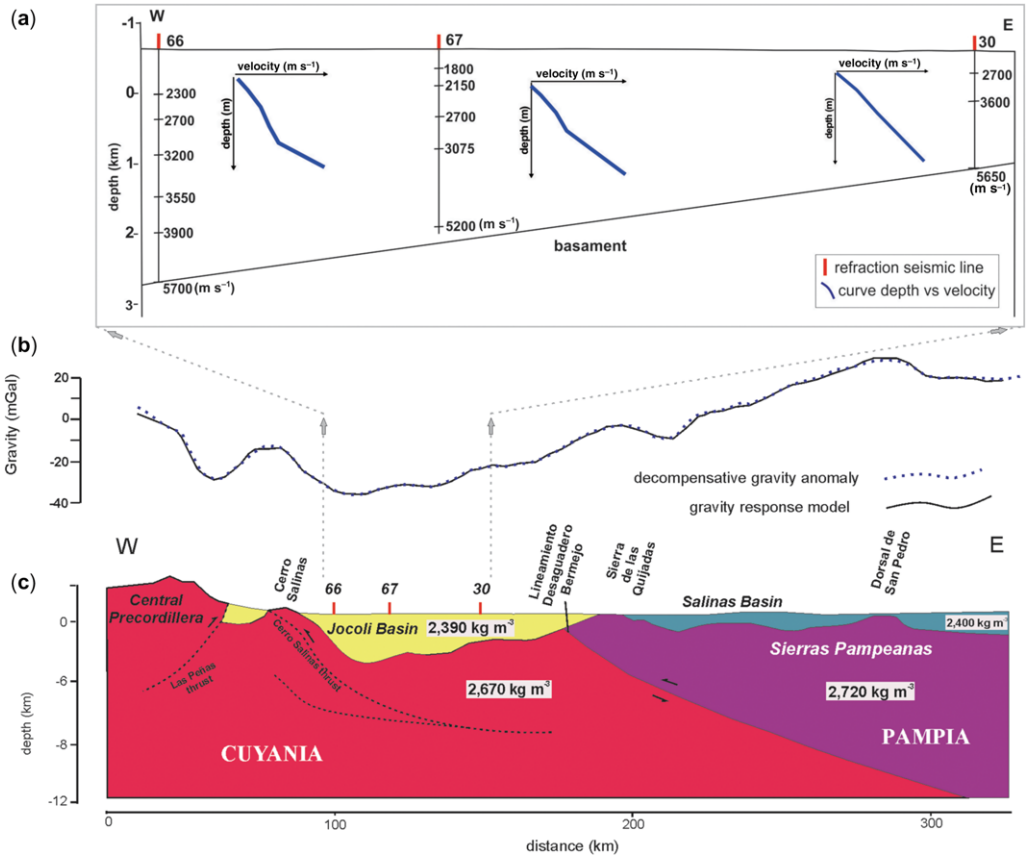

Fig. 9. Modelled Profile 1 from western Precordillera to eastern Sierras Pampeanas through the Sierra de las Quijadas. (**a**) The location of deep seismic refraction lines is shown in red and the velocities used to calculate densities from the Gardner equation are indicated in blue. (**b**) Fit between the decompensative gravity anomaly and the modelled profile. (**c**) Density model of the upper crust. The highest sedimentary thickness (*c*. 3000 m) is located in the Jocoli basin ($\rho_{\text{fill}} = 2390$ kg m^{-3}). Eastwards in the Western Sierras Pampeanas, a pronounced increase in the decompensative gravity anomaly has been linked to the contact zone between the basements of the Cuyania and Pampia terrains ($\rho = 2670$ kg m^{-3} v. $\rho = 2720$ kg m^{-3}). Pampia terrain constitutes the basement of the Salinas basin which has a sedimentary thickness of 1 km and a mean density of 2400 kg m^{-3} (Azeglio *et al.* 2010). See the text for more details.

Profile 2

This section extends for 300 km from the Eastern Precordillera to the western flank of the Sierra de San Luis in the Western Sierras Pampeanas, passing through the southern Jocoli basin and Sierra del Gigante (see location on Fig. 1b). The maximum sedimentary thickness of this basin is located to the eastern border of Central Precordillera as described in Profile 1, modelled with a density of 2670 kg m^{-3}. In this case the sediment thickness reaches up to 8000 m. The increasing depth of the Jocoli basin towards the Precordillera deformational front has been determined by Vergés *et al.* (2007) from a seismic section a few kilometres to the north (Fig. 10).

On the eastern-most region of this profile a high gravity value, potentially related to a density variation between the Cuyania and Pampia terrains, is observed in the Sierra del Gigante area. We do not discard a certain contribution to this density contrast derived from Early Cretaceous mafic bodies.

Results

The isostatic root found on the basis of the Airy–Heiskanen isostatic model (Fig. 3) shows a good correspondence with the Moho obtained by Gans *et al.* (2011) based on receiver functions and by Assumpção *et al.* (2013) based on active source experiments (deep seismic reflection surveys) and

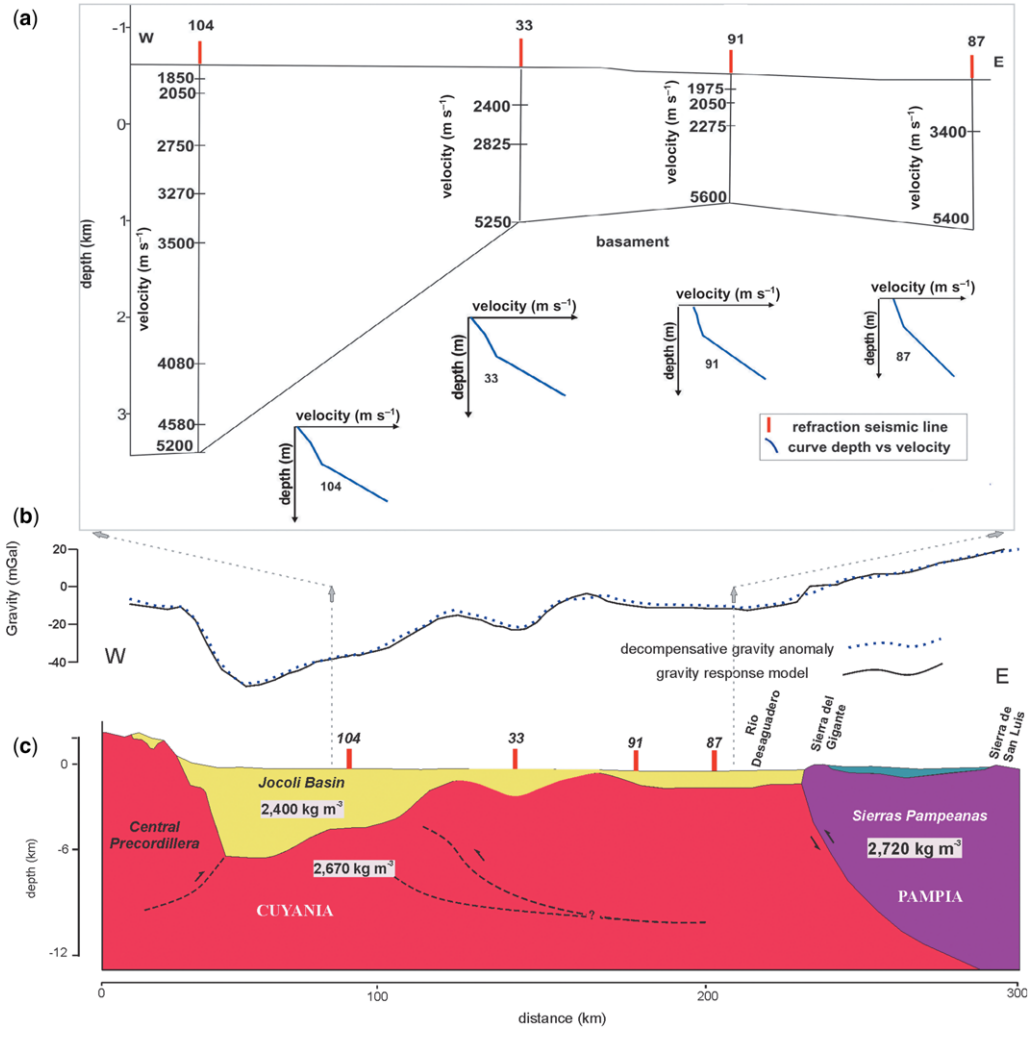

Fig. 10. Modelled Profile 2 from Precordillera to the western flank of the Sierra de San Luis in the Western Sierras Pampeanas. (**a**) The location of deep seismic refraction lines used as constraints is shown in red and velocities used to calculate densities from the Gardner equation are indicated in blue. (**b**) Fit between the decompensative gravity anomaly and the modelled profile. (**c**) Density model of the upper crust, where maximum sedimentary thicknesses reach up to 8000 m. On the easternmost region of this profile in the Sierra del Gigante area, a high gravity value is related to a density variation between the basements of the Cuyania and Pampia terrains.

receiver functions. The minimum values of the Bouguer anomaly (−300 mGal) found in Frontal Cordillera (Fig. 2) are related to the crustal thickening of *c.* 65 km obtained by the application of the Airy–Haiskenan local compensation model. These results are consistent with previous work. The gravity signal increases eastwards up to *c.* −50 mGal at Sierras Pampeanas, in relation to a progressive decrease in the crustal thickness to the foreland zone (45 km) (see Fig. 3). The gravity effect of the hydrostatic Moho (Fig. 4) behaves as a warped plane in which the eastern part corresponds to isoanomalies of the order −75 mGal, descreasing towards the west up to −225 mGal.

The isostatic anomaly map (Fig. 5) and the decompensative gravity anomaly (Fig. 7) are consistent with previous studies that are detailed below. Even though the figures are morphologically similar, the absolute scale and consequently the corresponding values vary. In the decompensative gravity anomaly map (Fig. 7), we identified different regions related to the main geological features:

(1) Frontal Cordillera (Introcaso *et al.* 1992*b*; Miranda & Robles 2002).
(2) The relative positive gravity response of the Precordillera within the general negative trend marked by the Andean root is clearly depicted (Introcaso *et al.* 1992*a*; Gimenez *et al.* 2000, 2009; Alvarez *et al.* 2012).
(3) The Jocoli basin, which is limited to the east by high anomalous values, is possibly associated with the continuity of the basement of Pie de Palo underneath (Martinez *et al.* 2008). The lowest values (−45 mGal) are localized towards the west, constituting evidence of the increase in sedimentary thickness towards the Precordillera deformational front.
(4) To the north of Sierra de San Luis, a high gravity value of more than 15 mGal is associated with a belt of mafic and ultra-mafic rocks with densities of the order 3000 kg m^{-3} (see Kostadinoff *et al.* 2010).
(5) The Cuyo basin with values of −30 mGal is linked to a sedimentary fill with density estimated as 2320 kg m^{-3} and thicknesses of 5 km (Miranda & Robles 2002).

Additionally, to enhance the anomalies related to density contrasts, we applied the Tilt method (Fig. 8). Areas of high gradients are indicated with warm colours, while cold colours indicate the sedimentary basins. Analysing the Tilt map, we can distinguish the following features.

(1) The Precordillera region is contoured by the contrast between the areas of warm and cold colours. This is in agreement with the decompensative gravity anomaly results.
(2) The Jocoli basin edges are depicted by the Tilt method, achieving a better resolution than in previous work (Fig. 7).
(3) The Bermejo–Desaguadero basin, an extensional basin associated with the reactivation of the boundary between Cuyania and Pampia terranes to the north, can be traced in the studied zone bordered by the Sierra de las Quijadas to the east. The Tilt method also highlights the San Pedro Ridge, a NW-oriented lineament of regional development (Kostadinoff *et al.* 2003; Kostadinoff & Gregori 2004; Azeglio *et al.* 2009). Even although this lineament cannot be related to a geological body with superficial expression, its presence is gravimetrically constrained; further work is necessary to understand its significance.
(4) Another important feature in this map is the high gradient located south of 33.4°S latitude, in a roughly NW direction. This is associated with the continuation of the Tunuyan lineament, identified east of 66.5°W by Kostadinoff & Gregori (2004). The Tunuyan lineament has been associated with a boundary between two regions with different seismotectonic behaviour (to the north, the Precordillera and to the south, the Southern Mendoza area) by Perucca & Bastias (2005). The seismotectonic behavioir has been associated with the transition zone between the flat subduction of the Nazca plate to the north and the segment of normal angle to the south (Perucca & Bastias 2005). Its real significance again merits further work, since it is transversal to the structural and gravimetric grain. Hypothetically, this feature could be related to some kind of crustal structure associated with the change in angle of the subduction zone or to an inherited basement structure.

Finally, results obtained by applying the Tilt method are consistent with the solutions found by Gimenez *et al.* (2008) when implementing the 3D Euler deconvolution method using gravity data.

Conclusions

The computed isostatic anomalies (Fig. 5) indicate that in the potential cessation of the dynamic forces that are sustaining the topography the Frontal Cordillera and Jocoli basin would ascend isostatically, while the Precordillera would ascend to a lesser extent. Contrastingly, the Sierra de San Luis and the Sierras Pampeanas to the foreland area should descend in order to reach isostatic equilibrium.

The decompensative gravity anomaly allows us to identify geological features such as Frontal Cordillera, Precordillera, Sierras Pampeanas, and the Cuyo and Jocoli basins. When applying the Tilt method, a technique that is used to highlight gravity anomalies associated with sources emplaced in the upper crust, the previously mentioned results are enhanced. Two regional lineaments are clearly delineated: San Pedro Ridge and the Tunuyan Lineament. The latter, located south of 33.4°S with an approximately NW orientation, coincides with morphological changes that occur in the subducted Nazca plate from flat to normal subduction angle.

The gravity models obtained from the decompensative gravity anomaly and constrained by the existing geological and geophysical data reveal the geometry of a segmented basement in the north of this region. Results obtained from both modelled profiles reveal that the basement deepens towards the Central Precordillera region. The depths of the modelled depocentres reach up to 8 km in the Jocoli basin and 2 km for the Salinas basin. To the foreland area, a significant increase in the residual

gravity anomaly could be due to the presence of high-density rocks associated with the closure of Palaeozoic ocean basins.

The authors acknowledge the use of the GMT-mapping software of Wessel & Smith (1998). We are also grateful to CONICET, Consejo Nacional de Investigaciones Científicas y Técnicas, Project PIP 6044, CICITCA, Project N°21 E901 and the Agencia Nacional de Promoción Científica y Tecnológica, Project PICT- 2007-01903 for their financial support.

References

Abbruzzi, J. M., Kay, S. M. & Bickford, M. E. 1993. Implications for the nature of the Precordilleran basement from the geochemistry and age of Precambrian xenoliths in Miocene volcanic rocks, San Juan province. *In*: *12° Congreso Geológico Argentino y 2° Congreso de Exploración de Hidrocarburos*, Buenos Aires, Actas, **3**, 331–339.

Aceñolaza, F. G., Miller, H. & Toselli, A. J. 2002. Proterozoic-Early Paleozoic evolution in western South America: a discussion. *Tectonophysics*, **354**, 121–137.

Allmendinger, R. W., Figueroa, D., Snyder, D., Beer, J., Mpodozis, C. & Isacks, B. L. 1990. Foreland shortening and crustal balancing in the Andes at 30° S Latitude. *Tectonics*, **9**, 789–809.

Almeida, F. F. M., Brito Neves, B. B. & Carneiro, C. D. R. 2000. The origin and evolution of the South American Platform. *Earth-Science Reviews*, **50**, 77–111.

Alvarado, P., Beck, S. & Zandt, G. 2007. Crustal structure of the south-central Andes Cordillera and backarc region from regional waveform modelling. *Geophysical Journal International*, **170**, 858–875.

Alvarez, O., Gimenez, M., Braitenberg, C. & Folguera, A. 2012. GOCE satellite derived gravity and gravity gradient corrected for topographic effect in the South Central Andes region. *Geophysical Journal International*, **190**, 941–941.

Assumpção, M., Bianchi, M. *et al.* 2013. Crustal thickness map of Brazil: data compilation and main features. *Journal of South American Earth Sciences*, **43**, 74e85.

Azeglio, E. A., Giménez, M. E. & Introcaso, A. 2009. La aplicación de técnicas de Señal Analítica a las estructuras de la cuenca de Las Salinas. *Revista de la Asociación Geológica Argentina*, **64**, 183–193.

Azeglio, E. A., Giménez, M. E. & Introcaso, A. 2010. Análisis estructural de la cuenca de Las Salinas y su relación con la acumulación de sedimentos eólicos en el área Médanos Negros. *Revista Asociación Geológica Argentina*, **67**, 2.

Baldis, B. A. & Chebli, G. 1969. Estructura profunda del área central de la Precordillera sanjuanina. *IV Jornadas Geologia Argentina*, **1**, 47–66. Argentina.

Baldis, B., Beresi, M., Bordonaro, O. & Vaca, A. 1982. Síntesis evolutiva de la Precordillera Argentina. *In*: *V Congreso Latinoamericano de Geología*, Buenos Aires, **IV**, 399445.

Benedetto, J. L. & Astini, R. A. 1993. A Collisional model for the stratigraphic evolution of the Argentine Precordillera during the Early Paleozoic. *In*: *2nd International Symposium on Andean Geodynamics*, Oxford, 501–504.

Benedetto, J. L., Sánchez, T. M., Carrera, M. G., Brussa, E. D. & Salas, M. J. 1999. Paleontological constraints on successive paleogeographic positions of Precordillera terrane during the early Paleozoic. *In*: Ramos, V. A. & Keppie, J. D. (eds) *Laurentia-Gondwana Connections before Pangea*. Geological Society, America, Special Paper, **336**, 21–42.

Bercowski, F., Ruzycki, L., Jordan, T., Zeitler, P., Caballero, M. M. & Perez, I. 1993. Litofacies y edad isotópica de la secuencia La Chilca y su significado paleogeográfico para el Neógeno de Precordillera. *In*: *Actas del 12° Congreso Geológico Argentino y 2° Congreso de Exploración de Hidrocarburos*, Mendoza, **1**, 212–217.

Blakely, R. 1995. *Potential Theory in Gravity and Magnetic Applications*. Cambridge University Press, Cambridge.

Boll, A. & de la Colina, J. 1993. Armazón estratigráfico del Triásico- Jurásico en Atamisqui-Cuenca Cuyana-Mendoza. *In*: *Actas XII Congreso Geológico Argentino y II Congreso de Exploración de Hidrocarburos*, Mendoza, Acta, **I**, 33–40.

Bracaccini, O. I. 1946. Contribución al conocimiento geológico de la Precordillera Sanjuanino-mendocina. *In*: *Boletín de Informaciones Petroleras*, Buenos Aires, 258–264.

Briggs, I. C. 1974. Machine contouring using minimum curvature. *Geophysics*, **39**, 39–48.

Brito Neves, B. B., Campos Neto, M. C. & Fuck, R. A. 1999. From Rodinia to Western Gondwana: an approach to the Brasiliano-Pan African cycle and orogenic collage. *Episodes*, **22**, 155–166.

Caminos, R. 1979. Sierras Pampeanas Noroccidentales Salta, Tucumán, Catamarca, La Rioja y San Juan. *Geología Regional Argentina, Academia Nacional de Ciencias, Córdoba*, **1**, 225–291.

Casquet, C., Pankhurst, R. J. *et al.* 2008. The Mesoproteroic Maz Terrane in the Western Sierras Pampeanas, Argentina, equivalent to the Arequipa-Antofalla block of southern Peru? Implications for West Gondwana margin evolution. *Gondwana Research*, **13**, 163–175.

Chapin, D. A. 1996. A deterministic approach toward isostatic gravity residuals-A case study from South America. *Geophysics*, **61**, 1022–1033.

Christensen, N. & Mooney, W. 1995. Seismic velocity structure and composition of the continental crust: a global view. *Journal of Geophysical Research*, **100**, 9761–9788.

Cominguez, A. H. & Ramos, V. A. 1990. Sísmica de reflección profunda entre Precordillera y Sierras Pampeanas. *In*: *XI Congreso Geológico Argentino*. San Juan. Actas, **II**, 311314.

Cominguez, A. H. & Ramos, V. A. 1991. La estructura profunda entre Precordillera y Sierras Pampeanas de la Argentina: evidencias de la sísmica de reflexión profunda. *Revista Geológica de Chile*, **18**, 3–14.

Cordell, L., Zorin, Y. A. & Keller, G. R. 1991. The decompensative gravity anomaly and deep structure

of the region of the Rio Grande rift. *Journal of Geophysical Research*, **96**, 6557–6568.

Figueroa, D. E. & Ferraris, O. R. 1989. Estructura del margen oriental de la Precordillera Mendocino-sanjuanina. *In*: *1° Congreso Nacional de Exploración de Hidrocarburos*, Mar del Plata, Buenos Aires, **1**, 515–529.

Finney, S. C., Gleason, J. D., Gehrels, G. G., Peralta, S. H. & Aceñolaza, G. 2003. Early Gondwana connection for the Argentina Precordillere Terrane. *Earth and Planetary Sciences Letters*, **205**, 349–359.

Galindo, C., Casquet, C., Rapela, C. W., Pankrurst, R. J., Baldo, E. & Saavedra, J. 2004. Sr, C, and O isotope geochemistry and stratigraphy of Precambrian and lower Paleozoic carbonate sequences from the western Sierras Pampeanas of Argentina: tectonic implications. *Precambrian Research*, **131**, 55–71.

Gans, C. R., Beck, S. L., Zandt, G., Gilbert, H., Alvarado, P., Anderson, M. & Linkimer, L. 2011. Continental and oceanic crustal structure of the Pampean flat slab region, western Argentina, using receiver function analysis: new high-resolution results. *Geophysical Journal International*, **186**, 45–58.

García Torrejón, M., Alvarez Pontoriero, O. *et al.* 2011. Evidencias de la zona de contacto entre los terrenos de Precordillera y Pie de Palo, Provincias de San Juan y Mendoza. *Revista de la Asociación Geológica Argentina*, **68**, 502–506.

Gardner, G. H. F., Gardner, L. W. & Gregory, R. 1974. Formation velocity and density – the diagnostic basis for stratigraphic traps. *Geophysics*, **39**, 770–780.

Gilbert, H., Beck, S. & Zandt, G. 2006. Lithosperic and upper mantle structure of Central Chile and Argentina. *Geophysical Journal International*, **165**, 383–398.

Gimenez, M. E., Martinez, M. P. & Introcaso, A. 2000. A Crustal Model based mainly on Gravity data in the Area between the Bermejo basin and the Sierras de Valle Fértil- Argentina. *Journal of South American Earth Sciences*, **13**, 275–286.

Gimenez, M., Martinez, P. & Introcaso, A. 2008. Determinaciones de lineamientos regionales del basamento cristalino a partir de un análisis gravimétrico. *Revista de la Asociación Geológica Argentina*, **63**, 288–296.

Gimenez, M. E., Braitenberg, C., Martinez, M. P. & Introcaso, A. 2009. A comparative analysis of Seismological and Gravimetric Crustal Thicknesses below the Andean Region with flat Subduction of the Nazca Plate. Hindawi Publishing Corporation International. *Journal of Geophysics*. Article ID 607458, http://dx.doi.org/10.1155/2009/607458

González Bonorino, F. 1950. Algunos problemas geológicos de las Sierras Pampeanas. *Revista de la Asociación Geológica Argentina*, **49**, 81110.

Götze, C. & Evans, B. 1979. Stress and temperature in the bending lithosphere as constrained by experimental rock mechanism. *Geophysical Journal of the Royal Astronomical Society*, **59**, 463–478.

Götze, H. J. & Kirchner, A. 1997. Interpretation of gravity and geoid in the Central Andes between 20° and 29° S. *Journal of South American Earth Sciences*, **10**, 179–188.

Hinze, W. J. 2003. Bouguer reduction density, why 2.67. *Geophysics*, **68**, 1559–1560.

Hinze, W. J., Aiken, C. *et al.* 2005. New standards for reducing gravity data: the North American gravity database. *Geophysics*, **70**, 4, J25–J32.

Introcaso, A. & Pacino, M. C. 1987. Gravity Andean model associated with subduction near 24°25′ south latitude. *Revista Geofísica*, **2**, 43.

Introcaso, A., Guspí, F., Robles, A., Martinez, P. & Miranda, S. 1992*a*. Carta gravimétrica de Precordillera y Sierras Pampeanas entre 30° y 32° de Latitud Sur. *In*: *17° Reunión de la Asociación Argentina de Geofísicos y Geodesias*, Buenos Aires.

Introcaso, A., Pacino, M. C. & Fraga, H. 1992*b*. Gravity, isostasy and Andean crustal shortening between latitudes 30° and 35° S. *Tectonophysics*, **205**, 31–48.

Introcaso, A., Pacino, M. C. & Guspi, F. 2000. The Andes of Argentina and Chile: Crustal configuration, Isostasy, Shortening and Tectonic features from Gravity Data. *Temas de Geociencia*, **5**, 31.

Kane, M. F. 1962. A comprehensive system of terrain corrections using a digital computer. *Geophysics*, **27**, 455–462.

Kay, S. M., Orrell, S. & Abbruzzi, J. M. 1996. Zircon and whole rock Nd-Pb isotopic evidence for a Grenville age and a Laurentian origin for the basement of the Precordilleran terrane in Argentina. *Journal of Geology*, **104**, 637–648.

Keller, M. 1999. Argentine Precordillera: Sedimentary and plate tectonic history of a Laurentian crustal fragment in South America. *Geological Society of America, Special Paper*, **341**, 134.

Kostadinoff, J. & Gregori, D. 2004. La Cuenca de Mercedes, provincia de San Luis. *Revista de la Asociación Geológica Argentina*, **59**, 488–494.

Kostadinoff, J., Bjerg, E., Raniolo, A. & Santiago, E. 2003. Anomalías del campo gravitatorio y magnético terrestre en la sierra de Socoscora, provincia de San Luis. *Revista de la Asociación Geológica Argentina*, **58**, 505–510.

Kostadinoff, J., Ferracutti, G. R. & Bjerg, E. A. 2010. Interpretación de una sección gravi-magnetométrica sobre la Pampa de las Invernadas, Sierra Grande de San Luis. *Revista de la Asociación Geológica Argentina*, **67**, 349–353.

Lagorio, S. L. 2008. Early Cretaceous alkaline volcanism of the Sierra Chica de Córdoba (Argentina): mineralogy, geochemistry and petrogénesis. *Journal of South American Earth Sciences*, **26**, 152–171.

Legarreta, L., Kokogian, D. & Dellape, D. 1993. Estructuración Terciaria de la Cuenca Cuyana. Cuánto de inversión tectónica? *Revista de la Asociación Geológica Argentina*, **47**, 83–86.

Llambías, E. J. 1966. Geología y petrografía del volcán Payún Matru. *Acta Geológica Lilloana*, **8**, 265–310.

Marquardt, D. 1963. An Algorithm for Least-Squares Estimation of Nonlinear Parameters. *SIAM Journal of Applied Mathematics*, **11**, 431–441.

Martinez, A., Rivarola, D., Strasser, E., Giambiagi, L., Roquet, M. B., Tobares, M. L. & Merlo, M. 2012. Petrografía y geoquímica preliminar de los basaltos cretácicos de la sierra de Las Quijadas y Cerrillada. *Serie Correlación Geológica*, **28**, 9–22.

MARTINEZ, M. P., GIMENEZ, M. E., BUSTOS, G., LINCE KLINGER, F., MALLEA, M. & JORDAN, T. 2006. Detección de Saltos de Basamento de la Cuenca del Valle de la Rioja-Argentina a partir de un Modelo Hidrostático. *GEOACTA*, **31**, 1–9.

MARTINEZ, M. P., GIMENEZ, M. E., INTROCASO, A. & RUIZ, F. 2007. Preliminary Geophysic Results in The Calingasta Bolson, Province of San Juan, Argentina. *In*: *U51B-01, AGU Meetings 2007*, Acapulco.

MARTINEZ, M. P., PERUCA, P. L., GIMENEZ, M. E. & RUIZ, F. 2008. Manifestaciones Geomorfológicas y Geoísicas de una Estructura Geológica al Sur de La Sierra de Pie de Palo. *Revista de la Asociación Geológica Argentina*, **63**, 104–111.

MILLER, H. G. & SINGH, V. 1994. Potential field tilt – A new concept for location of potential field sources. *Journal of Applied Geophysics*, **32**, 213–217.

MIRANDA, S. & INTROCASO, A. 1999. Cartas gravimétricas de la provincia de Córdoba, República Argentina: interpretación de la estructura profunda de la Sierra de Córdoba: Argentina, Universidad Nacional de Rosario. *Temas de Geociencia*, **1**, 45.

MIRANDA, S. & ROBLES, J. A. 2002. Posibilidades de atenuación cortical en la cuenca Cuyana a partir del análisis de datos de gravedad. *Revista de la Asociación Geológica Argentina*, **5**, 271–279.

MISHRA, D. C. & NAIDU, P. S. 1974. Two-dimensional power spectral analysis of aeromagnetic fields. *Geophysical Prospecting*, **22**, 345–353.

MOHR, P. J. & TAYLOR, B. N. 2001. The fundamental physical constant. *Physics Today*, **54**, 6–16.

MORELLI, C., GANTAR, C. *ET AL*. 1974. *The International Gravity Standardization Net 1971 (IGSN71)*. IUGG-IAG International Union of Geodesy and Geophysics, Special Publications, Paris, **4**.

MORITZ, H. 1980. Geodetic Reference System 1980. *Journal of Geodesy*, **54**, 395–405.

MULCAHY, S., ROESKE, S., MCCLELLAND, W., NOMADE, S. & RENNE, P. 2007. Cambrian initiation of the Las Pirquitas thrust of the western Sierras Pampeanas, Argentina: implications for the tectonic evolution of the proto-Andean margin of South America. *Geology*, **35**, 443–446.

NAGY, D. 1966. The gravitational attraction of a right rectangular prism. *Geophysics*, **31**, 362–371.

ORTIZ, A. & ZAMBRANO, J. J. 1981. La Provincia Geológica Precordillera Oriental. *In*: *VIII Congreso Geológico Argentino*, San Luis, Argentina, Actas, **III**.

ORUÇ, B. & SELIM, H. 2011. Interpretation of magnetic data in the Sinop area of Mid Black Sea, Turkey, using tilt derivative, Euler deconvolution, and discrete wavelet transform. *Journal of Applied Geophysics*, **74**, 194–204.

PANKHURST, R. J., RAPELA, C. W., SAAVEDRA, J., BALDO, E., DAHLQUIST, J., PASCUA, I. & FANNING, C. M. 1998. The Famatinian magmatic arc in the central Sierras Pampeanas: an Early to Mid- Ordovician continental arc on the Gondwana margin. *In*: PANKHURST, R. J. & RAPELA, C. W. (eds) *The Proto-Andean Margin of Gondwana*. Geological Society, London, Special Publication, **142**, 343–367.

PERALTA, S., PÖTHE DE BALDIS, E., LEÓN, L. & PEREYRA, M. 2003. Silurian of the San Juan Precordillera, western Argentina: stratigraphic framework. *In*: ORTEGA, G. & ACEÑOLAZA, G. F. (eds) *Proceedings of the 7° International Reappraisal of the Silurian Stratigraphy at Cerro del Fuerte section*, San Juan, Argentina INSUGEO, Serie Correlaciones Geológicas, **18**, 151–155.

PÉREZ-GUSSINYÉ, M., LOWRY, A. R., PHIPPS MORGAN, J. & TASSARA, A. 2008. Effective elastic thickness variations along the Andean margin and their relationship to subduction geometry. *Geochemistry Geophysics Geosystems*, **9**, Q02003, http://dx.doi.org/10.1029/2007GC001786

PERUCCA, L. & BASTIAS, H. 2005. El terremoto argentino de 1894: Fenómenos de licuefacción asociados a Sismos. Simp. Bodenender. INSUGEO. *Serie de Correlación Geológica*, **19**, 55–70.

QUENARDELLE, S. M. & RAMOS, V. A. 1999. Ordovician western Sierras Pampeanas magmatic belt: record of Precordillera accretion in Argentina. *In*: RAMOS, V. A. & KEPPIE, J. D. (eds) *Laurentia-Gondwana Connections before Pangea*. Geological Society of America, Boulder, Special Paper, **336**, 63–86.

RAMOS, V. A. 1988. The tectonics of the Central Andes; 30° to 33° S latitude. *In*: CLARK, S. & BURCHFIEL, D. (eds) *Processes in Continental Lithospheric Deformation*. Geological Society of America, Boulder, Special Paper, **218**, 31–54.

RAMOS, V. A. 1994. Terranes in Southern Gondwana land and their control in the Andean Structure (30°–33° latitude). *In*: REUTTER, K. J., SCHEUBER, E. & WIGGER, P. J. (eds) *Tectonics of the Southern Central Andes*. Springer-Verlag, New York, 249–261.

RAMOS, V. A. 1995. Sudamérica: un mosaico de continentes y océanos. *Ciencia Hoy*, **6**, 24–29.

RAMOS, V. A. 2004. Cuyania, an exotic block to Gondwana: review of a historical success and the present problems. *Gondwana Research*, **7**, 1009–1026.

RAMOS, V. A. & VUJOVICH, A. G. 1993. *Laurentia – Gondwana Connection: A South American Perspective*. GSA, Abstracts with Programs, Boston, **1**.

RAMOS, V. A., JORDAN, T. E., ALLMENDINGER, R., MPODOZIS, C., KAY, S. M., CORTES, J. M. & PALMA, M. 1986. Paleozoic terranes of the Central Argentine-Chilean Andes. *Tectonics*, **5**, 855–880.

RAMOS, V. A., CEGARRA, M. I., LO FORTE, G. & COMINGUEZ, A. 1997. El frente orogénico de la sierra de Pedernal (San Juan, Argentina): su migración a través de los depósitos sinorogénicos. *In*: *Actas 8° Congreso Geológico Chileno*, Chile, **3**, 1709–1713.

RAMOS, V. A., DALLMEYER, R. D. & VUJOVICH, G. 1998. Time constraints on the Early Palaeozoic docking of the Precordillera, central Argentina. *In*: *The Proto-Andean Margin of Gondwana*. Geological Society, London, Special Publications, **142**, 143–158.

RAMOS, V. A., CRISTALLINI, E. O. & PÉREZ, D. J. 2002. The Pampean Flat-Slab of the Central Andes. *Journal of South American Earth Sciences*, **15**, 59–78.

RAPALINI, A. E. & ASTINI, R. A. 1997. First Paleomagnetic Evidence for the Laurentian Origin of the Argentine Precordillera. *In*: *8th Scientific Assembly IAGA*, Uppsala, Sweden, Abstracts, 56.

RAPELA, C. W., PANKHURST, R. J. & FANNING, C. M. 2001. U-Pb SHRIMP ages of basement rocks from Sierra de la Ventana (Buenos Aires, Argentina).

In: *3rd South American Symposium on Isotope Geology*, Extended Abstracts (CD edition), Sociedad Geológica de Chile, Santiago, 225–228.

Rivarola, D. & Spalletti, L. 2006. Modelo de sedimentación continental para el rift cretácico de la Argentina central. Ejemplo de la Sierra de las Quijadas, San Luis. *Revista de la Asociación Geológica Argentina*, **61**, 63–80.

Rolleri, E. & Baldis, B. 1969. *Paleography and distribution of Carboniferous deposits in the Precordillera, Argentina*. La estratigrafía del Gondwana, Ciencias de la Tierra-2, Coloquio U.I.C.G. UNESCO, París (France).

Salem, A., Williams, S., Fairhead, D., Smith, R. & Ravat, D. 2008. Interpretation of magnetic data using tilt-angle derivatives. *Geophysics*, **73**, 1, doi: 10.1190/1.2799992.

Simpson, R. W., Jachens, R. C., Blakely, R. J. & Saltus, R. W. 1986. A new isostatic residual gravity map of the conterminous United States with a discussion on the significance of isostatic residual anomalies. *Journal of Geophysical Research*, **91**, 8348–8372.

Snyder, D. B., Ramos, V. A. & Allmendinger, R. W. 1990. Thick-skinned deformation observed on deep seismic reflection profiles in western Argentina. *Tectonics*, **9**, 773–788.

Somigliana, C. 1930. Geofisica – Sul campo gravitazionale esterno del geoide ellissoidico: Atti della Accademia nazionale dei Lincei. Rendiconti. *Classe di Scienze fisiche, Matematiche e Naturali*, **6**, 237–240.

Spector, A. & Grant, F. S. 1970. Statistical models for interpreting aeromagnetic data. *Geophysics*, **35**, 283–302.

Talwani, M., Worzel, J. L. & Landisman, M. 1959. Rapid gravity computations for two dimensional bodies with application to the Mendocino Submarine Fracture zone. *Journal of Geophysical Research*, **64**, 49–58.

Tassara, A. & Echaurren, A. 2012. Anatomy of the Andean subduction zone: three-dimensional density model upgraded and compared against global-scale models. *Geophysical Journal International*, **189**, 161–168.

Tassara, A. & Yáñez, G. 2003. Relación entre el espesor elástico de la litósfera y la segmentación tectónica del margen andino (15–478S). *Revista Geológica de Chile*, **30**, 159–186.

Tassara, A., Swain, C., Hackney, R. & Kirby, J. 2007. Elastic thickness structure of South America estimated using wavelets and satellite-derived gravity data. *Earth and Planetary Science Letters*, **253**, 17–36.

Thomas, W. A. & Astini, R. A. 2003. Ordovician accretion of the Argentine Precordillera terrane to Gondwana: a review. *Journal of South American Earth Sciences*, **16**, 67–79.

Thurston, J. B. & Smith, R. S. 1997. Automatic conversion of magnetic data to depth, dip and susceptibility contrast using the SPITM method. *Geophysics*, **62**, 807–813.

Uliana, M. A. & Biddle, K. T. 1988. Mesozoic-Cenozoic paleogeographic and geodynamic evolution of Southern South America. *Revista Brasileira de Geociencias*, **18**, 172–190.

Verduzco, B., Fairhead, J. D., Green, C. M. & MacKenzie, C. 2004. New insights into magnetic derivatives for structural mapping. *The Leading Edge*, **23**, 116–119.

Vergés, J., Ramos, V. A., Meigs, A., Cristallini, E., Bettini, F. H. & Cortés, J. M. 2007. Crustal wedging triggering recent deformation in the Andean thrust front between 31°S and 33°S: Sierras Pampeanas-Precordillera interaction. *Journal of Geophysical Research*, **112**, http://dx.doi.org/10.1029/2006JB004287

Villella, J. C. & Pacino, M. C. 2010. Interpolación gravimétrica para el cálculo de los números geopotenciales de la red altimétrica de Argentina en zonas de alta montaña. *GEOACTA*, **35**, 13–26.

von Gosen, W. 1992. Structural evolution of the Argentine Precordillera: the Río San Juan section. *Journal of Structural Geology*, **14**, 643–667.

Vujovich, G., Van Staal, C. R. & Davis, W. 2004. Age Constraints on the Tectonic Evolution and Provenance of the Pie de Palo Complex, Cuyania Composite Terrane, and the Famatinian Orogeny in the Sierra de Pie de Palo, San Juan, Argentina. *Gondwana Research*, **7**, 1041–1056.

Watts, A. B., Lamb, S. H., Fairhead, J. D. & Dewey, J. F. 1995. Lithospheric flexure and bending of the Central Andes. *Earth and Planetary Science Letters*, **134**, 9–20.

Wessel, P. & Smith, W. H. F. 1998. *New, improved version of the Generic Mapping Tools released*, Eos Trans. AGU, **79**, 579.

Whitman, D. 1999. Isostatic residual gravity anomaly in the Central Andes: 12 to 29 deg. S: A guide to interpreting crustal structure and deeper lithospheric processes. *International Geology Review*, **41**, 457–475.

Wienecke, S., Braitenberg, C. & Götze, H. J. 2007. A new analytical solution estimating the flexural rigidity in the Central Andes. *Geophysics Journal International*, **169**, 789–794.

Zapata, T. R. & Allmendinger, R. W. 1994. 'Thick-Skinned' Triangular zone of the Precordillera Thrust Belt, Argentina. *In*: *Canadian Society of Exploration Geophysicist and Canadian Society of Petroleum Geologist Joint National Convention*. Program with Expanded Abstracts and Bibliographies, 72–73.

Zapata, T. R. & Allmendinger, R. W. 1996. Thrust-front zone of the Precordillera, Argentina: a thick-skinned triangle zone. *AAPG Bulletin*, **80**, 359–381.

Zapata, T. R. & Allmendinger, R. W. 1997. Evolución de la deformación del frente de corrimiento de Precordillera, provincia de San Juan. *Revista de la Asociación Geológica Argentina*, **52**, 115–131.